Origin of Broad Emission Induced by Rigid Aromatic Ditopic Cations in Low-Dimensional Metal Halide Perovskites

Marta Morana,[a] Waldemar Kaiser,[b,] Rossella Chiara,[a] Benedetta Albini,[c] Daniele Meggiolaro,[b] Edoardo Mosconi,[b] Pietro Galinetto,[c] Filippo De Angelis,[b,d,e] Lorenzo Malavasi[a,*]*

[a]Department of Chemistry and INSTM, University of Pavia, Via Taramelli 16, Pavia, 27100, Italy

[b]Computational Laboratory for Hybrid/Organic Photovoltaics (CLHYO), Istituto CNR di Scienze e Tecnologie Chimiche "Giulio Natta" (CNR-SCITEC), 06123 Perugia, Italy

[c]Department of Physics, University of Pavia, Via Bassi 6, Pavia, 27100, Italy

[d]Department of Chemistry, Biology and Biotechnology, University of Perugia and INSTM, 06123 Perugia, Italy

[e]SKKU Institute of Energy Science and Technology (SIEST) Sungkyunkwan University, Suwon, Korea 440-746.

Corresponding Authors

Waldemar Kaiser, email: waldemar.kaiser@scitec.cnr.it;

Lorenzo Malavasi, email: lorenzo.malavasi@unipv.it; tel. +39 382 987921

ABSTRACT

The development of broadband emitters based on metal halide perovskites (MHPs) requires the elucidation of structure-emission property correlations. Herein, we report a combined experimental and theoretical study on a series of novel low-dimensional lead-chloride perovskites including ditopic aromatic cations. Synthesized lead-chloride perovskites and their bromide analogues show both narrow and broad photoluminescence emission properties as a function of the cation and halide nature. Structural analysis shows a correlation between the rigidity of the ditopic cations with the lead-halide octahedral distortions. Density functional theory calculations reveal, in turn, the pivotal role of octahedral distortions in the formation of self-trapped excitons which are responsible for the insurgence of broad emission and large Stokes shifts together with a contribution of halide vacancies. For the considered MHPs series the use of conventional octahedral distortion parameters allows to nicely describe the trend of emission properties thus providing a solid guide for further materials design.

2

Two-dimensional metal-halide perovskites (2D MHPs) have recently attracted great attention for application as light-absorbing and/or light-emitting materials, or as passivation layer on top of their 3D counterpart.[1–8] The inherently layered nature of 2D MHPs with A_2BX_4 chemical structure opens a tremendous construction kit made of A-site cations of various chemical building blocks, while the B- and X-site typically stick with traditional metal (B=Pb; Sn) and halide ions (X=I, Br, Cl), respectively.[9–13] While the optoelectronic properties are typically controlled by the inorganic scaffold, appropriate A-site cation engineering tailors MHPs stability and may modulate band alignment and its excitonic properties.[14–18] A-site cations can be distinguished by their charge, with monoammonium and diammonium cations being of most relevance for design of layered 2D MHPs.[11] While a large variety of monoammonium cations has already been demonstrated, diammonium cations as organic spacers in 2D MHPs are systematically underexplored.[11,19–21] Being ditopic ligands, such cations can directly interact with two separate inorganic layers. As for monoammonium cations, both linear and cyclic cations have been considered recently, suggesting a wide structural variability in diammonium-based 2D MHPs.[22–25] However, ditopic organic cations do not always lead to the formation of a layered perovskite structure but may also give rise to other topologies.

Linear diammonium cations of general formula $NH_3(CH_2)_mNH_3^{2+}$ with even carbon-chain lengths (m = 4, 8, 10, 12) form n = 1 2D lead-halide perovskites, while those with odd carbon chain length (m = 7) form 1D perovskitoid structures.[26] Moreover, diammonium cations with fused aromatic rings only give rise to 2D MHPs when being able to tilt in order to form hydrogen bonds to the halides.[27] In general, the tilting of diammonium cations seems to be of great importance, since aromatic cations, where the ammonium groups may have no degree of freedom, tend to form 1D perovskitoid motifs. This is the case for (4,4′-MDA)PbI$_4$ [MDA=methylenedianilinium] and (1,4-PDA)PbI$_4$ [PDA=phenylene-*p*-diammonium], while a similar but asymmetric diammonium cation *N,N*-dimethylphenylene-*p*-diamine (DPDA)

3

forms layered structure with both iodide and bromide but also 1D perovskitoids $(DPDA)_2PbI_5 \cdot I$ under different stoichiometric conditions.[24,27,28] Layered 2D MHPs were further reported for $(1,3\text{-PDA})PbBr_4$, $(1,4\text{-PDA})PbBr_4$, $(1,4\text{-XDA})PbBr_4$ (XDA=xylylenediammonium), together with $(1,3\text{-PDA})PbI_4$[29] and $(AEA)PbBr_4$ (AEA=3-(2-ammonioethyl)anilinium).[30,31] Heterocyclic diammonium cations such as 2,2'-biimidazolium, benzodiimidazolium, and 1,4-dimethylpiperazinium have also been reported, with the latter cation showing the 2D structure with n=1 for bromide compounds and 1D motifs with iodide.[32,33] A common feature of the 2D MHPs with ditopic cations is the relatively small interlayer distance due to their compact nature.[11]

2D MHPs incorporating diammonium cations not only show this rich and fascinating structural chemistry but also offer appealing functional properties for optoelectronic applications. Diammonium ligands have been considered in the photovoltaics field with, for example, the incorporation of propylenediammonium and trimethylenediammonium in $FASnI_3$ leading to improved film morphology and optoelectronic properties.[34] *Ortho-*, *meta-* and *para-*isomers of (phenylene)di(ethylammonium) iodide have been used as passivating layers in perovskite solar cells boosting the efficiency and long-term stability.[35] Recent reports showed improved charge transport properties using diammonium cations in 2D Dion-Jacobson (DJ) MHPs, likely caused by decreasing the gap between the 2D MHPs with charge transport layers.[36]

Even more interestingly, broadband white light emission has been observed in (*N*-MEDA)$PbBr_4$ (*N*-MEDA=N^1-methylethane-1,2-diammonium) and (EDBE)PbX_4 (EDBE=2,2′-(ethylenedioxy)bis(ethylammonium); X = Cl and Br), as well as for its tin-based counterpart (EDBE)SnI_4.[37,38] Recently, broadband emission was also observed in 2D lead bromide perovskites with ditopic aromatic cyclic cations, likely being correlated to the level of octahedral distortion.[30,39]

4

Still, the spectrum of available 2D MHPs with diammonium spacers remains limited with respect to their monoammonium counterparts. In addition, ditopic cations have been neglected so far in 2D lead-chloride perovskites with respect to their iodide and bromide counterparts. This hinders the comprehension of the role of structural degrees of freedom within the diammonium cations on both the resulting structural motifs (2D or 1D) and the functional properties. Understanding the latter is fundamental prerequisite to design novel and tailored diammonium-based 2D MHPs.

To provide a concise picture on the role of tuning the diammonium cation and the halide in 2D MHPs, we synthesize novel low-dimensional lead-chloride perovskites with four different aromatic diammonium cations (1,3-phenylenediammonium (1,3-PDA), 1,3-xylylenediammonium (1,3-XDA), 1,4-phenylenediammonium (1,4-PDA), and 1,4-xylylenediammonium (1,4-XDA)) and characterize their structural and optoelectronic properties in comparison with our previously synthesized 2D lead-bromide compounds.[30] 1,3-PDA, 1,4-PDA and 1,4-XDA result in 2D lead-chloride perovskites, whereas 1,3-XDA forms a 0D-perovskitoid structure. We interestingly observe significant differences in the light emission upon changing the diammonium cations and the halides, ranging from sharp emission close with energies to the absorption edge to broad, red-shifted light emission. Density functional theory (DFT) calculations demonstrate the correlation between the broad emission with the self-trapping of excitons inside the inorganic scaffold for the majority of 2D perovskites, while emission within the 0D perovskitoids $(1,3\text{-XDA})_2PbCl_6$ origins from the organic spacers itself. Sharp band-to-band emission is only observable for the $(1,4\text{-XDA})PbBr_4$ showing lowest octahedral distortions, in which self-trapping of excitons is absent in our theoretical calculations. Our results reveal a direct relation between the structural and the optoelectronic properties of diammonium-based low dimensional perovskites, providing design rules for novel 2D MHPs with tailored optoelectronic properties.

Single crystals of the four lead-chloride compounds with 1,3-PDA, 1,4-PDA, 1,3-XDA and 1,4-XDA have been grown (see Experimental Section in Supporting Information, SI) and characterized by single-crystal x-ray diffraction (chemical structures reports in Figure S1 of Supporting Information, SI). The resulting crystal structures and chemical formulas are reported in Table 1. Note that 1,3-PDA and 1,4-PDA have been previously used in preparing chloride perovskites reporting only the crystal structure without any further characterization of optical or electronic properties.[25] According to Table 1, the prepared compounds show different structure types, as depicted in Figure 1.

Table 1. Crystal structure data for A_nPbCl_m samples (A= 1,3-PDA, 1,3-XDA, 1,4-PDA, and 1,4-PDA).

Sample	Chemical formula	S.G. and Volume ($Å^3$)	a,b,c (Å)	α, β, γ (°)
$(1,3\text{-PDA})PbCl_4$	$(1,3\text{-}C_6H_{10}N_2)PbCl_4$	P2/c Monoclinic 1223.18(13)	20.4867(11) 8.4386(5) 7.0834(5)	90 92.735(6) 90
$(1,3\text{-XDA})_2PbCl_6$	$(1,3\text{-}C_8H_{14}N_2)_2PbCl_6$	$P2_1/c$ Monoclinic 1192.13(13)	10.5995(7) 13.8588(7) 8.3131(5)	90 102.518(7) 90
$(1,4\text{-PDA})Pb_2Cl_6$	$(1,4\text{-}C_6H_{10}N_2)Pb_2Cl_6$	$P2_1/c$ Monoclinic 777.53(8)	13.7789(8) 7.8328(4) 7.4805(4)	90 105.622(6) 90
$(1,4\text{-XDA})PbCl_4$	$(1,4\text{-}C_8H_{14}N_2)\,PbCl_4$	*Pnma* Orthorhombic 1467.31(10)	7.7006(3) 24.3807(9) 7.8154(3)	90 90 90

6
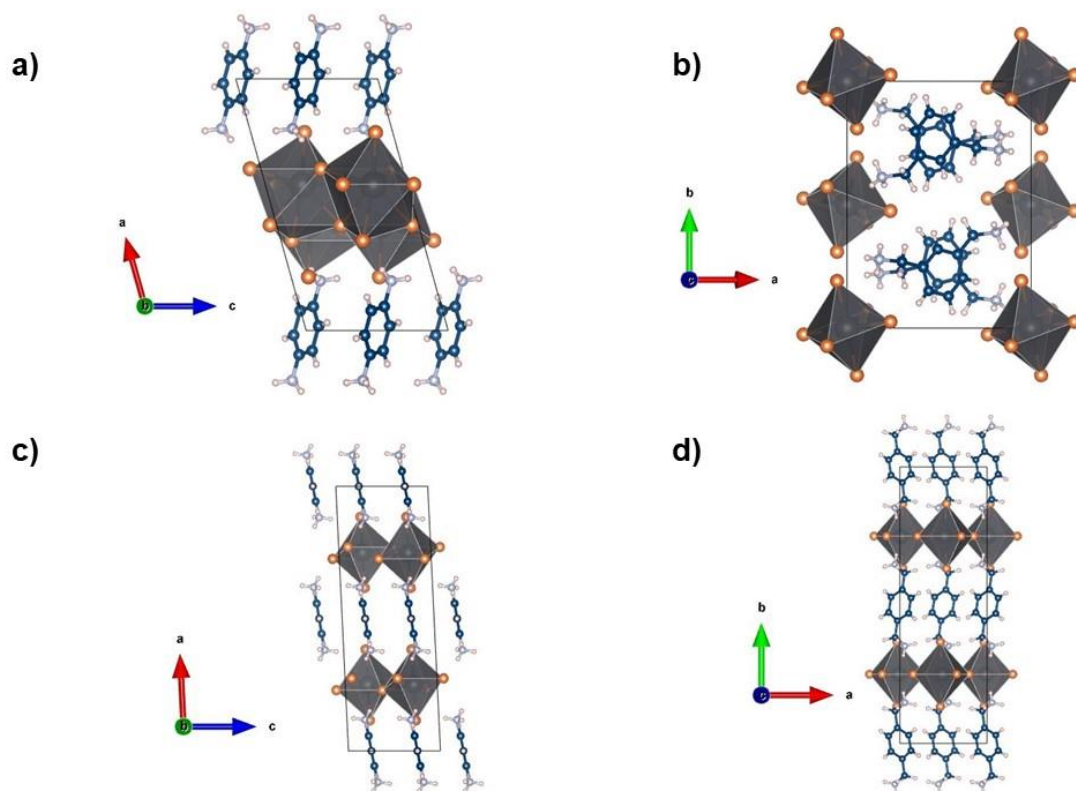
Figure 1 Crystal structures of a) $(1,3\text{-PDA})PbCl_4$, b) $(1,3\text{-XDA})_2PbCl_6$, c) $(1,4\text{-PDA})Pb_2Cl_6$, d) $(1,4\text{-XDA})PbCl_4$.

$(1,3\text{-XDA})_2PbCl_6$ does not have a layered structure but corresponds to a so-called 0D perovskitoid being constituted by isolated octahedra. Notably, it is isostructural to $(1,3\text{-XDA})_2PbBr_6$, suggesting that the 1,3-XDA cation may have a large tendency to form this topology.[30] This structure type is probably not common with diammonium cations, even if other chloride containing 0D systems have been reported in the past.[25] $(1,4\text{-PDA})Pb_2Cl_6$ shows a layered structure, with an inorganic layer made of face-sharing square antiprisms and a layer of organic cations located on the inversion center. The central Pb atom is eight-fold coordinated with Pb–Cl distances ranging from 2.8029(18) to 3.3869(15), creating a distorted square antiprism. The structure described in this work is in very good agreement with previous works, for which optical data were note reported.[25,40] On the other hand, $(1,3\text{-PDA})PbCl_4$ and $(1,4\text{-XDA})PbCl_4$ crystallize as 2D Dion-Jacobson (DJ) phases with $n=1$ comprising layers of $PbCl_6$ octahedra separated by layers of organic cations. It is well known

7

that the interaction between the ammonium group and the octahedral framework deeply affects the structure and properties of layered perovskites.[9,10] A useful parameter to explore this effect is the penetration depth, which is the distance between the N atom of the amino group and the plane of the terminal halides.[20] The NH_3^+ penetration influences both the inter-octahedral, in terms of the X-Pb-X angle, and intra-octahedral distortion parameters, in terms of octahedral elongation length ($\langle \lambda_{oct} \rangle$) and bond angle variance (σ_{oct}^2).[30,41] In particular, considering for comparison the bromide and chloride containing phenylamines reported so far, some general trends can be envisaged (Figure 2a). With the same organic cation, the penetration depth increases from the chloride to the bromide perovskites, probably as a consequence of the different strength of the hydrogen bond. [20,42,43] The position and length of the substituents seems to play a role: 1,3-PDA cations have shorter depth of penetration, most likely because of the steric hindrance of the relatively close substituents, while the 1,4-PDA and 1,4-XDA cations have larger penetration and more regular octahedral layers. Among them, 1,4-PDA gives rise to the largest tilting, *i.e.* smallest X-Pb-X angle, since it is short and rigid and has less degrees of freedom, whilst the 1,4-XDA cation has longer substituents that can more easily interact with the halide.
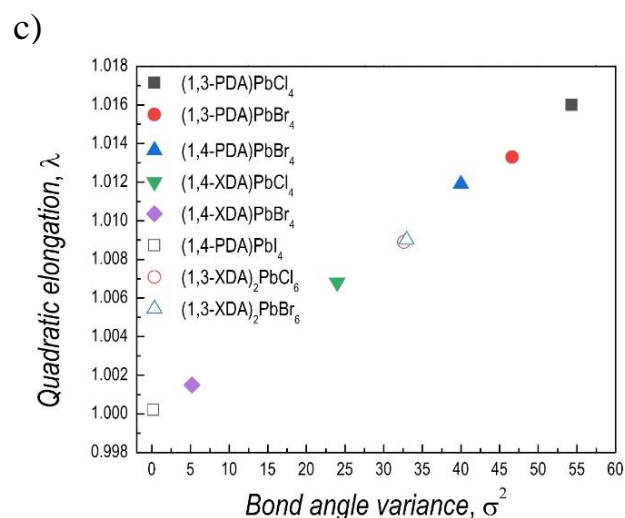

8

c)
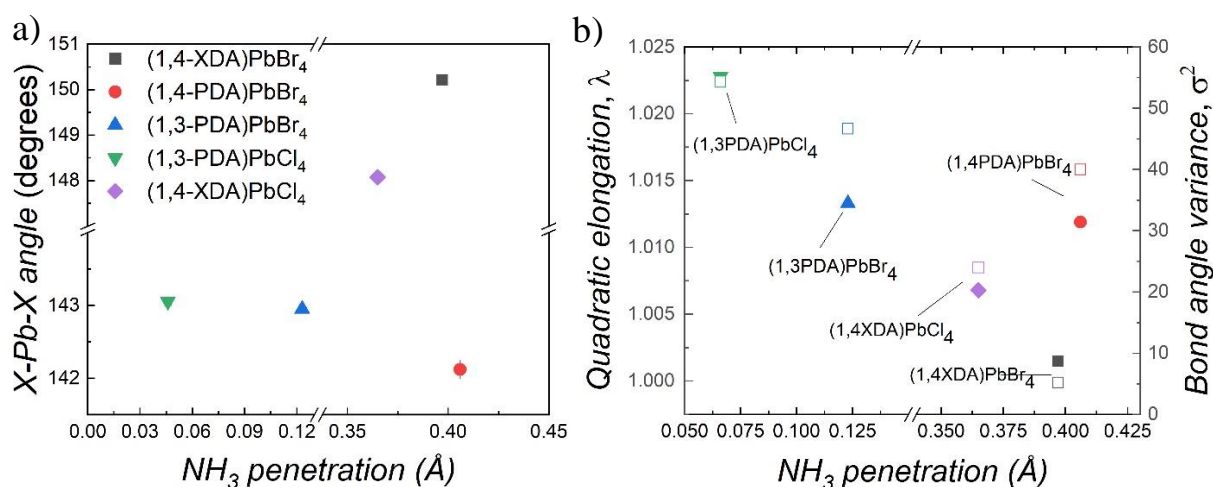
Figure 2: a) X-Pb-X angle and b) octahedral elongation and bond angle variance as a function of NH_3 penetration for chloride and bromide compositions crystallizing in 2D perovskites; c) Octahedral elongation as a function of bond angle variance. PDA= phenylenediammonium and XDA= xylylenediammonium.

Similar but opposite trends can also be seen in the intra-octahedral distortion parameters (Figure 2b). In fact, the 1,3-PDA cations have small NH_3 penetration, but give rise to large distortions within the octahedra. Among the 1,4 cations, the rigidity of 1,4-PDA again seems to affect the PbX_6 octahedra, inducing a distortion close to the one found for the 1,3-PDA cations. On the other hand, the more flexible 1,4-XDA cations allow for more regular octahedra. When the same organic cation is involved, the distortion within the octahedra increases with the hardness of the halide from Br to Cl, as predicted by first-principles calculations[44] and shown by local structure studies[45,46]. Finally, in order to have further insight into the role of the flexibility of the organic cation, we extend the analysis of the intra-octahedral distortion including all the compounds with available crystal structure even if not showing a layered perovskite structure (Figure 2c). It is worth noting that the smallest distortion is shown by $(1,4-PDA)PbI_4$ where symmetry constrains together with the edge sharing motif present in the structure give rise to regular lead-iodide octahedra.[24] Then, the XDA cations have an increasing distortion, with 1,3-XDA cations generating a larger but very

9

close distortions, supporting the idea that the 0D arrangement is mostly due to the type of organic cation. The more rigid PDA cations, and in particular the 1,3 ones, induce the largest distortions within the octahedra. Furthermore, as already pointed out, the distortion increases with the hardness of the halide passing from iodide to bromide and chloride. Based on these results, it is clear that, among the low-dimensional perovskites including the four ditopic cations considered in this work, the chloride samples show the highest degree of distortion which may have a relevant effect on the optical properties.
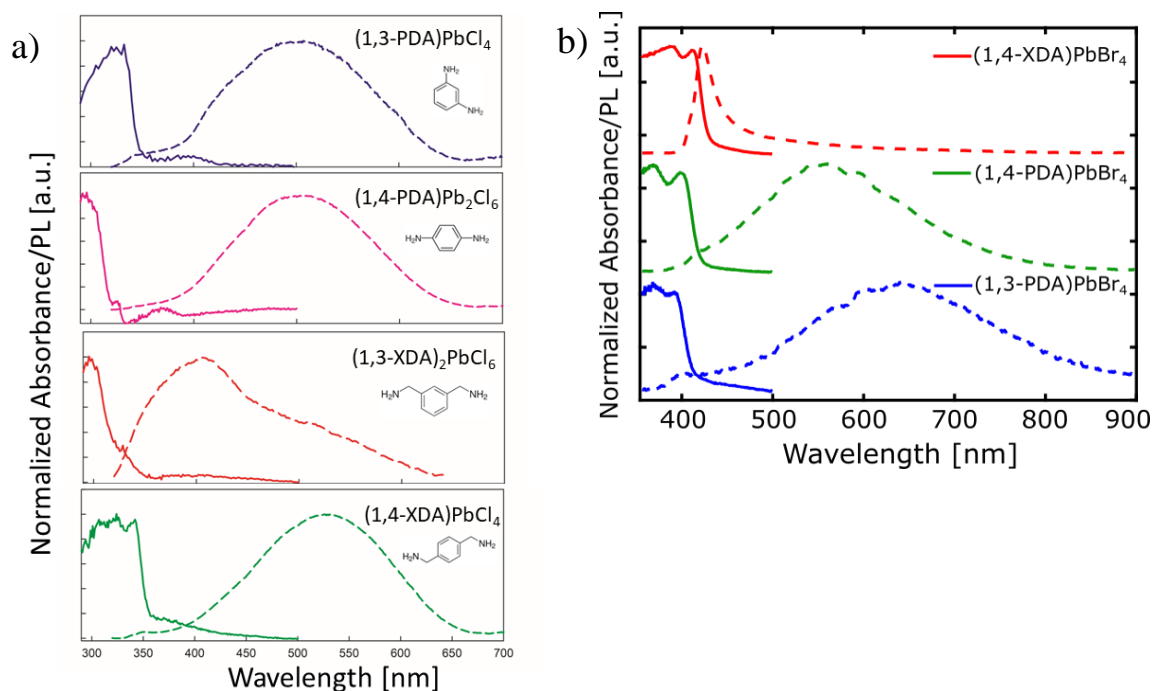

Figure 3: a) Absorption (solid lines) and PL (dashed lines) spectra of $(1,3PDA)PbCl_4$ (blue line), $(1.4 PDA)Pb_2Cl_6$ (purple line), $(1,3 XDA)_2PbCl_6$ (red line), and $(1,4 XDA)PbCl_4$ (green line) at RT.; b) Absorption (solid lines) and PL (dashed lines) spectra of $(1,4XDA)PbBr_4$ (red line), $(1.4 PDA)PbBr_4$ (green line), and $(1,3 PDA)PbBr_4$ (blue line) at RT.[30] All spectra are acquired using an excitation wavelength, λ_{ex}, at 300 nm

The optical properties of the four chloride-based samples are investigated by room temperature absorption and PL measurements, which are reported in Figure 3a. The absorbance (solid lines), calculated from the reflectivity of powdered single crystals, shows an

10

absorption edge for the four samples in the range between 300 nm and 360 nm, an expected value for 2D lead-chloride perovskites.[11,47–50] From these measurements the band gaps of the four samples have been determined: 3.53 eV for $(1,3\text{-PDA})PbCl_4$, 3.92 eV for $(1,4\text{-PDA})Pb_2Cl_6$, 3.87 eV for $(1,3\text{-XDA})_2PbCl_6$, and 3.51 eV for $(1,4\text{-XDA})PbCl_4$. A clear blue-shift in the band gap is observed for non-perovskite structures which is due to confinement effects in the electronic structure of the inorganic scaffold, while for $(1,3\text{-PDA})PbCl_4$ and $(1,4\text{-XDA})PbCl_4$ the close values confirm that the main contribution of halide and lead in the band edges remain unchanged upon exchange of the cation, as confirmed by our DFT calculations, see Figure S2, Supporting Information.

The static PL (dashed lines) in Figure 3a, measured under an excitation at 300 nm, commonly shows a substantially red-shifted broad emission for $(1,3\text{-PDA})PbCl_4$, $(1,4\text{ -}PDA)Pb_2Cl_6$, and $(1,4\text{-XDA})PbCl_4$, extending in most of the visible spectrum, with peaks centered at 503, 506, and 525 nm, respectively, and FWHMs around 200 nm. For $(1,3\text{-XDA})Pb_2Cl_6$, on the other hand, an asymmetric PL with a peak centered around 410 nm, followed by a longer tail, is found. Moreover, for the previous three samples, a very large Stokes shift of more than 200 nm is observed, while for the latter, $(1,3 \text{ XDA})Pb_2Cl_6$, the Stoke shift is around 100 nm. Broadband emission has been observed in few chloride perovskites including monoammonium cations and in just one composition including a diammonium cations, namely 3-aminopyrrolidinium (displaying a (110)-oriented 2D perovskite structure).[31,48–51] Finally, the role of the halide on the distortion, and in turn on the emission behavior, can be isolated by comparing the bromide and chloride analogues that form 2D DJ perovskites. The spectroscopic measurements carried out previously by our group on the bromide analogues, namely $(1,3\text{-PDA})PbBr_4$, $(1,4\text{-PDA})PbBr_4$, $(1,4\text{-XDA})PbBr_4$, are reproduced in Figure 3b to allow a direct comparison.[30] Both bromide and chloride sample including 1,3-PDA display a broadband emission, in agreement with the high distortion induced by this cation. On the other hand, a transition from narrow to broad emission is

11

observed when moving from (1,4-XDA)PbBr$_4$ to (1,4-XDA)PbCl$_4$. Looking at the PL spectra, the majority of investigated perovskites show a substantial Stokes shift. The only exception is (1,4-XDA)PbBr$_4$, showing a sharp PL peak at 420 nm and a broad but less intense peak centered at around 600 nm.

In literature, broad emission is often attributed to either self-trapped excitons or emission from defect states, typically halide vacancies, while a clear connection to their structural properties is still under debate.[51–54] Our experimental PL data of a broad range of materials with similar structural moieties may allow further insight into the nature of the broad emission features in 2D MHPs. DFT calculations are performed to rationalize the origin of the broad emission, distinguishing emission from self-trapped excitons (STE) and halide vacancies, V$_X$. The energy of STE emission is calculated by the difference between the energies of the triplet and singlet states, $E^{T1}(STE)$ and $E^{S0}(STE)$, respectively, calculated at the equilibrium geometry of the STE, see schematic representation in Figure 4:

$$PL(STE) = E^{T1}(STE) - E^{S0}(STE)$$

Emission from halide vacancies is given by

$$PL(V_X) = \varepsilon(+/0) - [E^+(V_X^0) - E^+(V_X^+)]$$

with thermodynamic ionization level $\varepsilon(+/0)$, the energy of the positively charged supercell at V_X^+ and V_X^0 equilibrium geometry. Further computational details are given in the Supporting Information.
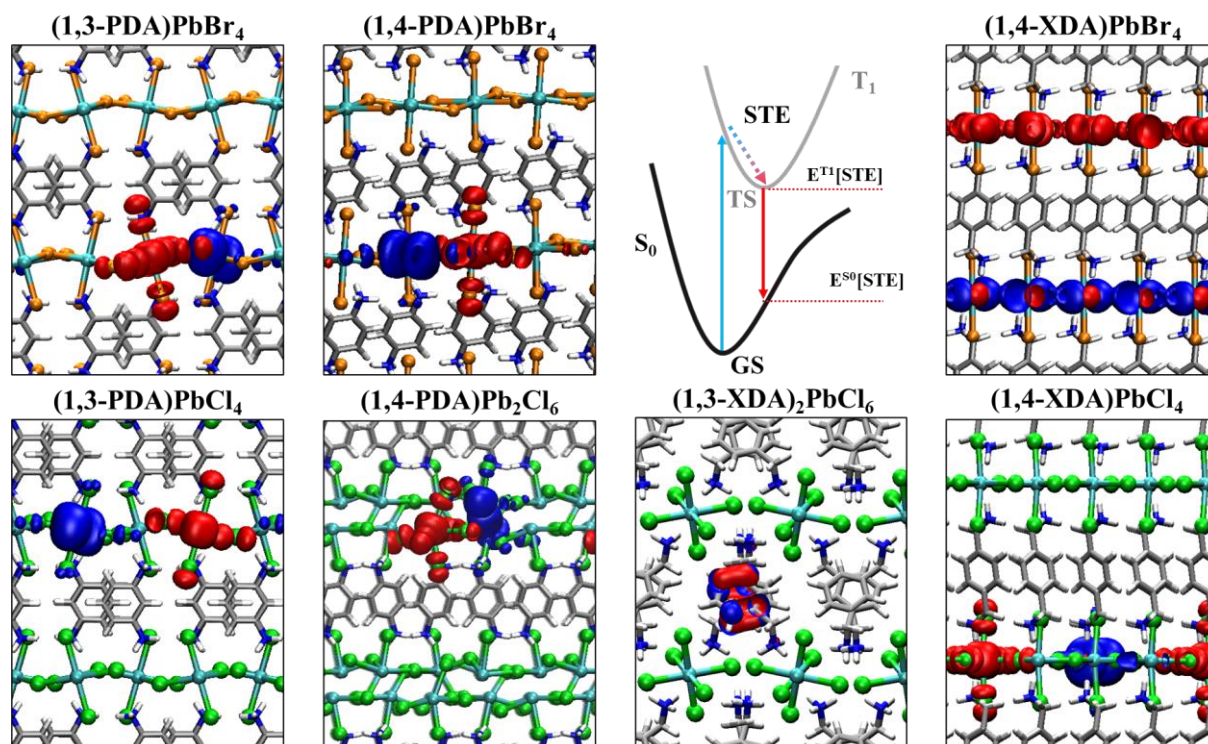
12

Figure 4. Visualization of electron (blue) and hole (red) Kohn-Sham (KS) orbitals for diammonium-based low dimensional MHPs after geometry relaxation in the excited triplet state. The Jablonski diagram in the upper row visualizes the formation mechanism of self-trapped excitons and the red-shifted PL emission from the STE to the potential energy surface of the ground state. (1,4-XDA)PbBr$_4$ shows delocalized states along the inorganic scaffold; in (1,3-XDA)$_2$PbCl$_6$, the triplet state localizes within the 1,3-XDA cation; self-trapping of excitons is observed in all remaining compounds.

We obtain an excellent agreement between the theoretical values of PL emission energies from STE and the experimental ones for a large set of perovskites, in particular (1,3-PDA)PbBr$_4$, (1,4-PDA)PbBr$_4$, (1,3-PDA)PbCl$_4$, (1,4-PDA)Pb$_2$Cl$_6$, (1,3-XDA)$_2$PbCl$_6$ and (1,4-XDA)PbCl$_4$, see Table 2. Emission from halide vacancies show comparable energy values, Table 2, likely contributing to the broad emission of all investigated perovskites. Note that for (1,3-XDA)$_2$PbCl$_6$ STE localizes within the organic cations, as the electronic states of the carbon moieties dominate the conduction band edge of the given 0-D perovskitoid, see Figure S3c and Figure S4, SI. In the remaining perovskites, STEs form within the inorganic lead-halide scaffold, see Figure 4. Despite the structural similarity, the (1,4-XDA)PbBr$_4$ does not show STE formation. Self-trapping of excitons requires a certain distortion of the inorganic scaffold, which appears less likely due to the reduction of octahedral tilting in (1,4-XDA)PbBr$_4$, see Figure 2. Comparing all bromide-based 2D MHPs, no substantial differences

13

in the electronic structure in the electronic ground state is observed, see Figure S2. We consequently assign the sharp PL peak at 420 nm to band-to-band emission of delocalized excitons. Furthermore, the presence (absence) of STE may be attributed to a large (low) octahedral tilting, providing an indicator for a rapid screening of potential material candidates for broad emitters. Our results further suggest that the strong red-shift is dominated by differences in the singlet energies between the ground state and the STE geometry, causing a substantial relaxation upon emission, see Table 2.

Based on our results, we may hypothesize on the nature of broad emission when having different spectral features. The presence of a sharp emission peak is due to band-to-band emission of delocalized excited states. Systems with sharp emission still may show broad emission features, but with low intensity, due to halide vacancies. Consequently, defect passivation may reduce the broad emission, in line with recent reports.[55] In case of STE formation, being favored by octahedral tilting, the sharp emission peak vanishes while a broad, Stokes shifted emission peak raises strongly. Emission from STE or from halide vacancies likely contribute both to the broad emission features, while the formation of STEs is required to design broad emitters. Note that the presence of Stokes shifted broad emission in the absence of STE would require an enormous defect density. Considering the relatively sharp absorption edges, see Figure 3, halide vacancies alone may not cause, but certainly contribute to, the experimentally observed broad emission Stokes shifted emission features. Finally, we want to point out that the simple structural parameters σ^2 and λ_{oct}, reported in Figure 2 for the present samples are excellent descriptors for an efficient screening of potential candidates for broad emission in line with previous reports.[51,56,57]

14

Table 2. Emission energies for diammonium-based perovskites with bromide and chloride as halide ions. Experimental PL energies are extracted from UV-vis spectra, and theoretical values are obtained from DFT calculations distinguishing emission from self-trapped excitons (STEs) and halide vacancies V_X (X=Br, Cl) in equatorial (eq) and in apical (ap) position. Energy differences in the singlet (S_0) and triplet states (T_1) are reported, with TS and GS representing the relaxed geometries in the triplet and singlet states, respectively, see Figure 4. ΔSOC represents the correction term to account for spin-orbit coupling effects due to the heavy Pb ions. Theoretical band gap energies are summarized in Table S2, Supporting Information, for completeness.

* Sharp emission peak due to band-to-band emission; no self-trapped excitons observed.

** Emission from 1,4-XDA cation.

[a] refers to equatorial and apical vacancies, respectively

Perovskite	PL emission	T_1(@GS)-GS	S_0(@TS)-GS	TS-T_1(@GS)	ΔSOC	Theory	
						STE	**Vx** [a]
(1,3-PDA)PbBr$_4$	1.9	3.73	1.13	0.34	0.37	1.89	2.21/2.50
(1,4-PDA)PbBr$_4$	2.2	3.76	1.01	0.14	0.51	2.10	2.11/2.40
(1,4-XDA)PbBr$_4$	3.0*	3.67	0.06	0.03	-	-	1.76/1.76
(1,3-PDA)PbCl$_4$	2.5	4.44	1.50	0.51	0.25	2.18	2.34/2.29
(1,4-PDA)Pb$_2$Cl$_6$	2.4	4.78	1.61	0.58	0.24	2.35	2.94/2.67
(1,3-XDA)$_2$PbCl$_6$	3.0	4.03	1.23	0.22	-	2.96**	2.77/2.69
(1,4-XDA)PbCl$_4$	2.4	4.24	1.22	0.22	0.36	2.44	2.24/2.19

15

Herein, we reported a series of novel low-dimensional lead-chloride perovskites including four different monoammonium cations, namely (1,3-PDA), (1,3-XDA), (1,4-PDA), and (1,4-XDA). Their crystal structure, elucidated by single-crystal x-ray diffraction, allowed to expand the actual comprehension of the role of ditopic cation and halide nature on the distortion of the inorganic framework and their light emission properties, including in this correlation also bromide analogues previously synthesized by our group.[30] Based on this solid structure-property correlation, we provide tuning strategies to move from narrow emission, with small Stokes shift, to broadband emitters with Stokes shifts of the order of 150-200 nm. The mechanism underpinning the different nature of the emission has been elucidated by DFT calculations. Narrow emission has been correlated to band-to-band emission of delocalized excited states with low-intensity broad emission caused by halide vacancies. On the other hand, broadband emission has been unambiguously associated to the STE formation, in turn closely related to octahedral tilting, with a possible minor contribution to these spectral features of halide vacancies which, however, cannot account, alone, for the observed broad emission. Based on this extended combined experimental and computational modelling work we conclude that, for bromide and chloride low-dimensional perovskites including a rigid ditopic cation, the description, and therefore modulation, of their emission properties can be realized by playing with the σ^2 and λ_{oct} structural parameters. The present paper provides a solid base for the future design of broadband emitters which are triggering a huge interest due to their potential use as single emitters in optoelectronic devices.

16

Declaration of interests

The authors declare no competing interests.

Supplemental Information

Supporting Information Available: Materials and Methods; Computational details.

Acknowledgement

References

1 Y. Zhang and N.-G. Park, *ACS Energy Lett.*, 2022, **7**, 757–765.

2 W. Fu, J. Wang, L. Zuo, K. Gao, F. Liu, D. S. Ginger and A. K.-Y. Jen, *ACS Energy Lett.*, 2018, **3**, 2086–2093.

3 H. Tsai, W. Nie, J.-C. Blancon, C. C. Stoumpos, R. Asadpour, B. Harutyunyan, A. J. Neukirch, R. Verduzco, J. J. Crochet, S. Tretiak, L. Pedesseau, J. Even, M. A. Alam, G. Gupta, J. Lou, P. M. Ajayan, M. J. Bedzyk, M. G. Kanatzidis and A. D. Mohite, *Nature*, 2016, **536**, 312–316.

4 H. Ren, S. Yu, L. Chao, Y. Xia, Y. Sun, S. Zuo, F. Li, T. Niu, Y. Yang, H. Ju, B. Li, H. Du, X. Gao, J. Zhang, J. Wang, L. Zhang, Y. Chen and W. Huang, *Nat. Photonics*, 2020, **14**, 154–163.

5 L. Zhang, C. Sun, T. He, Y. Jiang, J. Wei, Y. Huang and M. Yuan, *Light Sci Appl*, 2021, **10**, 61.

6 P. Pang, G. Jin, C. Liang, B. Wang, W. Xiang, D. Zhang, J. Xu, W. Hong, Z. Xiao, L. Wang, G. Xing, J. Chen and D. Ma, *ACS Nano*, 2020, **14**, 11420–11430.

7 G. Grancini, C. Roldán-Carmona, I. Zimmermann, E. Mosconi, X. Lee, D. Martineau, S. Narbey, F. Oswald, F. De Angelis, M. Graetzel and M. K. Nazeeruddin, *Nat Commun*, 2017, **8**, 15684.

8 G. Wu, R. Liang, M. Ge, G. Sun, Y. Zhang and G. Xing, *Advanced Materials*, 2022, **34**, 2105635.

9 D. B. Mitzi, *J. Chem. Soc., Dalton Trans.*, 2001, 1–12.

10 B. Saparov and D. B. Mitzi, *Chem. Rev.*, 2016, **116**, 4558–4596.

11 X. Li, J. M. Hoffman and M. G. Kanatzidis, *Chem. Rev.*, 2021, **121**, 2230–2291.

12 L. Mao, C. C. Stoumpos and M. G. Kanatzidis, *J. Am. Chem. Soc.*, 2019, **141**, 1171–1190.

13 J. Zhao, Z. Zhang, G. Li, M. H. Aldamasy, M. Li and A. Abate, *Advanced Energy Materials*, 2023, **13**, 2204233.

14 C. Katan, N. Mercier and J. Even, *Chem. Rev.*, 2019, **119**, 3140–3192.

15 T. Ishihara, J. Takahashi and T. Goto, *Solid State Communications*, 1989, **69**, 933–936.

16 A. Mahata, E. Mosconi, D. Meggiolaro and F. De Angelis, *Chem. Mater.*, 2020, **32**, 105–113.

17 J. Yin, H. Li, D. Cortecchia, C. Soci and J.-L. Brédas, *ACS Energy Lett.*, 2017, **2**, 417–423.

18 E. Mosconi, A. A. Alothman, R. Long, W. Kaiser and F. De Angelis, *ACS Energy Lett.*, 2023, **8**, 748–752.

19 D. G. Billing and A. Lemmerer, *Acta Crystallogr B Struct Sci*, 2007, **63**, 735–747.

20 K. Du, Q. Tu, X. Zhang, Q. Han, J. Liu, S. Zauscher and D. B. Mitzi, *Inorg. Chem.*, 2017, **56**, 9291–9302.

21 M.-H. Tremblay, J. Bacsa, B. Zhao, F. Pulvirenti, S. Barlow and S. R. Marder, *Chem. Mater.*, 2019, **31**, 6145–6153.

22 G. A. Mousdis, G. C. Papavassiliou, C. P. Raptopoulou and A. Terzis, *J. Mater. Chem.*, 2000, **10**, 515–518.

23 Y. Han, Y. Li, Y. Wang, G. Cao, S. Yue, L. Zhang, B. Cui and Q. Chen, *Adv. Optical Mater.*, 2020, **8**, 1902051.

24 A. Lemmerer and D. G. Billing, *Acta Cryst C*, 2006, **62**, m597–m601.

25 L. Dobrzycki and K. Woźniak, *CrystEngComm*, 2008, **10**, 577–589.

26 A. Lemmerer and D. G. Billing, *Dalton Trans.*, 2012, **41**, 1146–1157.

27 A. Lemmerer and D. G. Billing, *CrystEngComm*, 2012, **14**, 1954–1966.

18

28 M. P. Hautzinger, J. Dai, Y. Ji, Y. Fu, J. Chen, I. A. Guzei, J. C. Wright, Y. Li and S. Jin, *Inorg. Chem.*, 2017, **56**, 14991–14998.

29 L. Gao, X. Li, B. Traoré, Y. Zhang, J. Fang, Y. Han, J. Even, C. Katan, K. Zhao, S. Liu and M. G. Kanatzidis, *J. Am. Chem. Soc.*, 2021, **143**, 12063–12073.

30 R. Chiara, M. Morana, G. Folpini, A. Olivati, B. Albini, P. Galinetto, L. Chelazzi, S. Ciattini, E. Fantechi, S. A. Serapian, A. Petrozza and L. Malavasi, *J. Mater. Chem. C*, 2022, **10**, 12367–12376.

31 M. D. Smith, A. Jaffe, E. R. Dohner, A. M. Lindenberg and H. I. Karunadasa, *Chem. Sci.*, 2017, **8**, 4497–4504.

32 Z. Tang, J. Guan and A. M. Guloy, *J. Mater. Chem.*, 2001, **11**, 479–482.

33 I. Zimmermann, S. Aghazada and M. K. Nazeeruddin, *Angew. Chem. Int. Ed.*, 2019, **58**, 1072–1076.

34 W. Ke, C. C. Stoumpos, I. Spanopoulos, M. Chen, M. R. Wasielewski and M. G. Kanatzidis, *ACS Energy Lett.*, 2018, **3**, 1470–1476.

35 C. Liu, Y. Yang, K. Rakstys, A. Mahata, M. Franckevicius, E. Mosconi, R. Skackauskaite, B. Ding, K. G. Brooks, O. J. Usiobo, J.-N. Audinot, H. Kanda, S. Driukas, G. Kavaliauskaite, V. Gulbinas, M. Dessimoz, V. Getautis, F. De Angelis, Y. Ding, S. Dai, P. J. Dyson and M. K. Nazeeruddin, *Nat Commun*, 2021, **12**, 6394.

36 M. D. Malouangou, Y. Yang, Y. Zhang, L. Bai, J. T. Matondo, M. Tabu Mbumba, M. Waleed Akram and M. Guli, *Energy Tech*, 2022, **10**, 2101155.

37 M. D. Smith and H. I. Karunadasa, *Acc. Chem. Res.*, 2018, **51**, 619–627.

38 E. K. Tekelenburg, N. Aledlbi, L. Chen, G. R. Blake and M. A. Loi, *J. Mater. Chem. C*, 2023, 10.1039.D2TC04626A.

39 P. Fu, M. A. Quintero, C. Welton, X. Li, B. Cucco, M. C. De Siena, J. Even, G. Volonakis, M. Kepenekian, R. Liu, C. C. Laing, V. Klepov, Y. Liu, V. P. Dravid, G. N. Manjunatha Reddy, C. Li and M. G. Kanatzidis, *Chem. Mater.*, 2022, **34**, 9685–9698.

40 S. A. Bourne and Z. Mangombo, *CrystEngComm*, 2004, **6**, 438–442.

41 K. Robinson, G. V. Gibbs and P. H. Ribbe, *Science*, 1971, **172**, 567–570.

42 T. Steiner, *Acta Crystallographica Section B*, 1998, **54**, 456–463.

43 L. Brammer, E. A. Bruton and P. Sherwood, *Crystal Growth & Design*, 2001, **1**, 277–290.

44 U. V. Waghmare, N. A. Spaldin, H. C. Kandpal and R. Seshadri, *Phys. Rev. B*, 2003, **67**, 125111.

45 G. Laurita, D. H. Fabini, C. C. Stoumpos, M. G. Kanatzidis and R. Seshadri, *Chemical Science*, 2017, **8**, 5628–5635.

46 M. Morana, J. Wiktor, M. Coduri, R. Chiara, C. Giacobbe, E. L. Bright, F. Ambrosio, F. De Angelis and L. Malavasi, *J. Phys. Chem. Lett.*, 2023, **14**, 2178–2186.

47 C. Lermer, A. Senocrate, I. Moudrakovski, T. Seewald, A.-K. Hatz, P. Mayer, F. Pielnhofer, J. A. Jaser, L. Schmidt-Mende, J. Maier and B. V. Lotsch, *Chem. Mater.*, 2018, **30**, 6289–6297.

48 Z. Wu, C. Ji, Z. Sun, S. Wang, S. Zhao, W. Zhang, L. Li and J. Luo, *J. Mater. Chem. C*, 2018, **6**, 1171–1175.

49 X. Li, P. Guo, M. Kepenekian, I. Hadar, C. Katan, J. Even, C. C. Stoumpos, R. D. Schaller and M. G. Kanatzidis, *Chem. Mater.*, 2019, **31**, 3582–3590.

50 K. Thirumal, W. K. Chong, W. Xie, R. Ganguly, S. K. Muduli, M. Sherburne, M. Asta, S. Mhaisalkar, T. C. Sum, H. S. Soo and N. Mathews, *Chem. Mater.*, 2017, **29**, 3947–3953.

51 S. Kahmann, D. Meggiolaro, L. Gregori, E. K. Tekelenburg, M. Pitaro, S. D. Stranks, F. De Angelis and M. A. Loi, *ACS Energy Lett.*, 2022, **7**, 4232–4241.

52 E. P. Booker, T. H. Thomas, C. Quarti, M. R. Stanton, C. D. Dashwood, A. J. Gillett, J. M. Richter, A. J. Pearson, N. J. L. K. Davis, H. Sirringhaus, M. B. Price, N. C. Greenham, D. Beljonne, S. E. Dutton and F. Deschler, *J. Am. Chem. Soc.*, 2017, **139**, 18632–18639.

53 S. Kahmann, E. K. Tekelenburg, H. Duim, M. E. Kamminga and M. A. Loi, *Nat Commun*, 2020, **11**, 2344.

54 Q. Zhang, Y. Ji, Z. Chen, D. Vella, X. Wang, Q.-H. Xu, Y. Li and G. Eda, *J. Phys. Chem. Lett.*, 2019, **10**, 2869–2873.

55 J. Yin, R. Naphade, L. Gutiérrez Arzaluz, J.-L. Brédas, O. M. Bakr and O. F. Mohammed, *ACS Energy Lett.*, 2020, **5**, 2149–2155.

56 M. D. Smith, B. A. Connor and H. I. Karunadasa, *Chem. Rev.*, 2019, **119**, 3104–3139.

57 X.-B. Han, C.-Q. Jing, H.-Y. Zu and W. Zhang, *J. Am. Chem. Soc.*, 2022, **144**, 18595–18606.